Comments on Inorganic Chemistry
Publication details, including instructions for authors and subscription information:
http://www.informaworld.com/smpp/title~content=t713455155

Photoelectron Spectroscopy

To cite this Article (1984) 'Photoelectron Spectroscopy', Comments on Inorganic Chemistry, 3: 5, 272 — 287
To link to this Article: DOI: 10.1080/02603598408080077
URL: http://dx.doi.org/10.1080/02603598408080077

(b) J. E. Hahn, M. S. Co, D. J. Spira, K. O. Hodgson, and E. I. Solomon, Biochem. Biophys. Res. Comm. **112**, 737–745 (1983).
(c) V. W. Hu, S. I. Chan, G. S. Brown, Proc. Nat. Acad. Sci. USA **74**, 3821–3825 (1977).
(d) J. M. Brown, L. Powers, B. Kincaid, J. A. Larrabee, and T. B. Spiro, J. Am. Chem. Soc. **102**, 4210–4216 (1980).
7. J. E. Hahn, R. A. Scott, K. O. Hodgson, S. Doniach, S. R. Desjardins and E. I. Solomon, Chem. Phys. Lett., **88**, 595–598 (1982).
8. (a) C. A. Bates, W. S. Moore, K. J. Standley, and K. W. H. Stevens, Proc. Phys. Soc. **79**, 73 (1962).
(b) M. Sharnoff, J. Chem. Phys. **42**, 3383 (1965).
9. J. E. Penner-Hahn, K. O. Hodgson, and E. I. Solomon, manuscript in preparation.
10. R. A. Bair and W. A. Goddard, Phys. Rev. **B22**, 2767 (1980).
11. T. A. Smith, M. Berding, J. E. Penner-Hahn, S. Doniach, and K. O. Hodgson, manuscript in preparation.

VI. PHOTOELECTRON SPECTROSCOPY

A. Basic Principles

Photoelectron spectroscopy (PES) provides a powerful probe of the energy level diagram of a metal complex, down to binding energies on the order of 1000 eV (Figure VI-1).[1] This method complements the methods discussed in preceding sections in that rather than measuring the energy and number of photons absorbed due to excitation of electrons into unoccupied bound states or the continuum, PES measures the kinetic energy (E_k) and number of electrons ejected upon photoexcitation into the continuum (referred to as photoemission). For a photon of fixed energy $h\nu$, the kinetic energy of the ejected electron is given by the Einstein relation,

$$E_k = h\nu - E_B. \tag{VI-1}$$

Most research in PES is directed toward determining the binding energies (E_B) of electrons in the energy levels of a metal complex. Usually, the photon sources available for PES have fixed values of $h\nu$ and thus photoelectron spectroscopy is subdivided into two fields, XPS (x-ray photoelectron spectroscopy) and UPS (ultraviolet photoelectron spectroscopy), based on the type and thus energy regime of the source used. (With the availability of continuously tunable synchrotron radiation, this distinction is becoming less clear.)

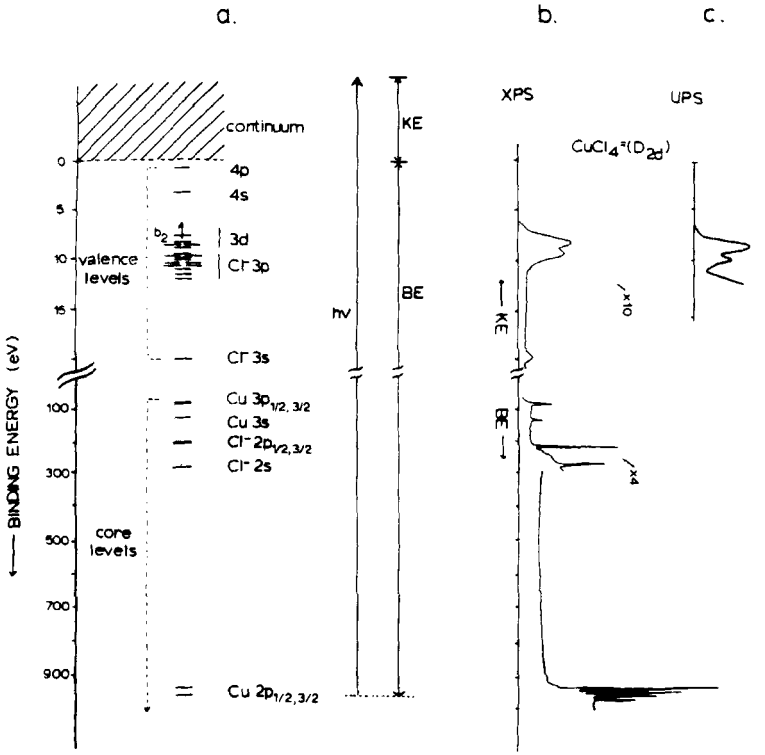

FIGURE VI-1 Energy level diagram and PES spectra of D_{2d}–$CuCl_4^=$: (a) Lower lying core and valence levels filled to the half-occupied b_2 level. $p_{1/2,\,3/2}$ indicates spin orbit splitting of the core level ($l = 1$; $j = 3/2, 1/2$). (b) XPS spectrum using 1253.6 eV source. As indicated to the right in (a), higher kinetic energy = lower binding energy. (c) UPS spectrum using 48.4 eV source.

In x-ray photoelectron spectroscopy[2] (XPS) an x-ray anode producing photons of 1253.6 eV (Mg$K\alpha$) or 1486.7 eV (Al$K\alpha$) is employed. These photons are of high enough energy to ionize core electrons into the continuum. In $CuCl_4^=$, the core levels accessible with these photon energies include Cu 2s (1099 eV), Cu $2p_{1/2,3/2}$ (933, 953 eV), Cu 3s (123 eV), Cu $3p_{1/2,3/2}$ (77 eV), Cl 2s (270 eV), Cl $2p_{1/2,3/2}$ (200, 202 eV) (Figure VI-1b). Core level photoelectron peaks are generally observed to shift to deeper binding energy with increasing oxidation state of the atom. This is known in XPS as a chemical shift and can be used to determine the oxidation state or

charge density on an atom in a molecule.[2a] Considering the example of the 3*s* core level in $CuCl_4^=$ (Figure VI-2), reduction from Cu(II) to Cu(I) produces a shift of ~1.5 eV to lower binding energy for the photoelectron peak.[3]

The binding energy of the core peak is also sensitive to the presence of unpaired electrons in the valence orbitals. Ejection of a photoelectron from the Cu 3*s* level leaves one unpaired electron ($s = ½$) which can couple with the unpaired electron ($s = ½$) in the half-occupied $d_{x^2-y^2}$ orbital. These spins interact through electron repulsion to produce a singlet and a triplet state which are split by an amount given by the Van Vleck expression for photoemission from a filled *s* level,

$$\Delta E = \frac{2S + 1}{2l + 1} K(s,l) \qquad \text{(VI-2)}$$

where S is the spin of the ground state, l is the orbital angular momentum of the valence shell and $K(s,l)$ is the exchange integral.[4]

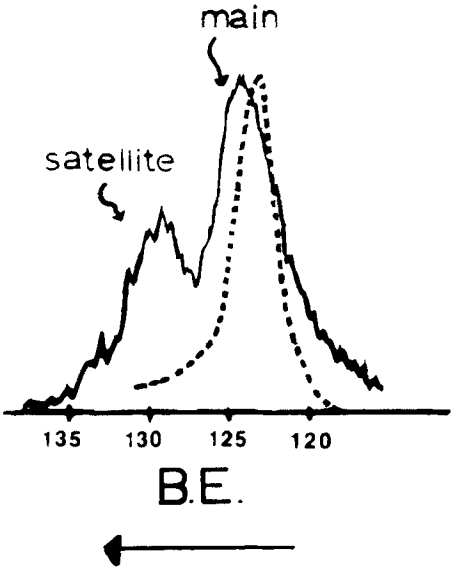

FIGURE VI-2 XPS spectrum of Cu 3*s* core level in D_{2d}-$Cu(II)Cl_4^=$: Dashed line for $Cu(I)Cl_4^{3-}$ estimated from Ref. 3a.

Thus, this multiplet splitting of the 3*s* level (which is observed[3] as an unresolved broadening of the peak by ~1 eV, Figure VI-2) gives a direct quantitative measure of the exchange interaction of a 3*d* electron with the 3*s* core. It should be emphasized that this interaction is also responsible for the spin polarization of core electrons which produces the isotropic contribution to hyperfine splitting of the EPR spectrum (see Section VII).

Finally, the XPS spectrum can also provide information which relates to the charge–transfer transitions discussed in Section IV. In $CuCl_4^=$, an additional peak is observed in the Cu 3*s* spectrum at ~7 eV to deeper binding energy than the main peak[3] (Figure VI-2). This is a satellite or shake-up peak[5] which corresponds to simultaneous 3*s* photoemission and excitation of a valence electron from the Cl 3*p* levels into the half occupied $d_{x^2-y^2}$ orbital. While this is formally a two-electron transition and the electric dipole moment operator can induce only one-electron transitions, the transition becomes allowed through configurational interaction (CI) with the one-electron 3*s* photoemission peak. Thus the satellite feature is a charge-transfer transition of the ionized complex with the appropriate symmetry for CI mixing with the main peak. As the symmetry of this shake-up transition will in general be different from that allowed in electronic absorption spectroscopy, satellite structure provides a complementary low resolution probe of metal-ligand bonding.

Electrons in valence orbitals can also be studied using XPS (see high KE part of spectrum in Figure VI-1b), however, this can be accomplished at higher resolution (Figure VI-1c) using ultraviolet photoelectron spectroscopy[6] (UPS). In UPS, photons produced by a dc (or microwave) discharge source generally have energies below 50 eV, the most common being the He I line at 21.2 eV and the He II line at 40.8 eV. These photon energies are capable of ionizing electrons from the valence Cu 3*d* and Cl 3*p* (and Cl 3*s*) levels, thus the separation between photoelectron peaks will, in principle, probe the same bonding interactions which were studied by electronic absorption spectroscopy in the ligand-field and charge-transfer regions as discussed in Section III and IV. Figure VI-3 compares[7] parallel UPS and optical spectral regions for the D_{2d}–$CuCl_4^=$ in Cs_2CuCl_4. Clearly, electronic absorption spectroscopy provides much more detail in probing the splittings of the metal and ligand orbitals due to bonding. However, the UPS spectrum provides complementary information in that the widths of the entire Cl 3*p* and Cu 3*d* bands are observed

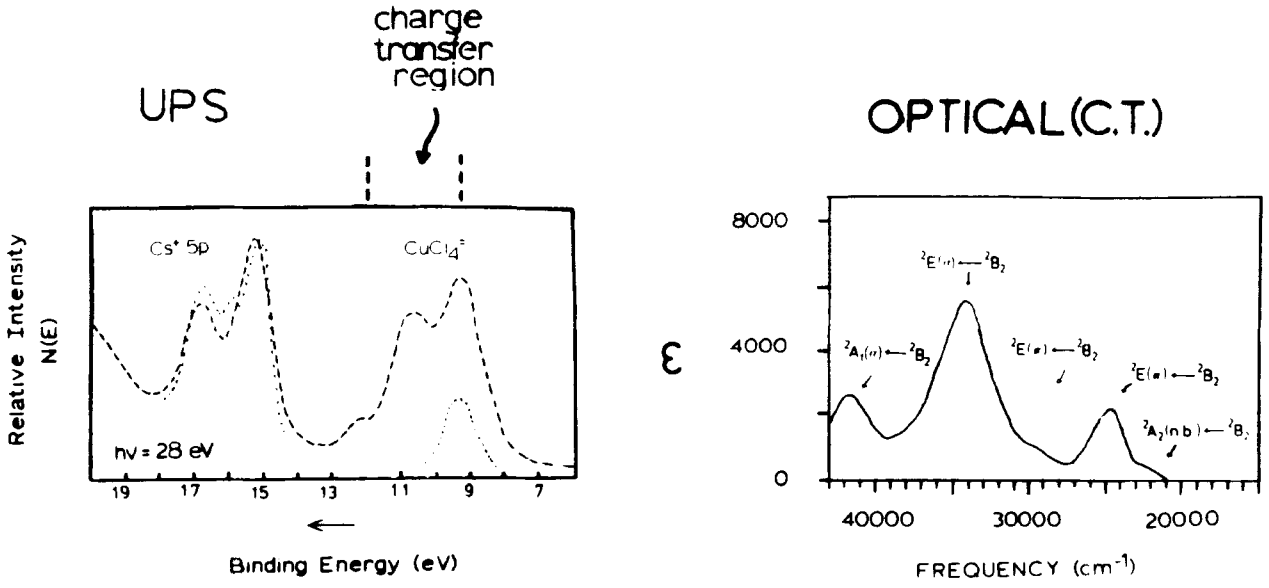

FIGURE VI-3 Comparison of charge transfer region of UPS and optical spectra of D_{2d}–$CuCl_4^=$. Note that the UPS spectrum of CsCl has been included as a reference (dotted line).

since selection rules allow ionization from all $CuCl_4^=$ molecular orbitals. In addition, if one is interested in probing the bonding of $Cu(I)Cl_4^{3-}$, the d^{10} closed shell precludes the possibility of low energy electronic absorption transitions. However, the UPS spectrum of the $Cu(I)Cl_4^{3-}$ complex will again provide the relative energy level ordering of the Cu 3*d* and Cl 3*p* levels (*vide infra*). Thus, x-ray absorption spectroscopy (Section V) and PES are the main spectroscopic probes of bonding interactions in closed-shell systems.

Finally, it should be emphasized that applying different spectroscopic techniques to evaluate a one-electron energy level diagram, such as the one pictured in Figure VI-1, is quite approximate. This approach ignores differences in electron-electron repulsion and orbital relaxation (the latter leading to deviations from Koopmans' Theorem in a Hartree-Fock SCF molecular orbital description) that are involved in each type of spectroscopy and which depend on the localization properties of the orbitals involved in the transition.[4] Thus the effective energy level diagrams derived from UPS or optical absorption spectroscopy will not necessarily be the same. Figure VI-4 compares transition state SCF-Xα-SW calculations (which take these factors into account) for the electronic absorption and UPS specta of D_{2d}–$CuCl_4^=$, where the ground state of the complex $^2B_2(5b_2)$ and of the ionized complex $^1A_1(5b_2)$ have been aligned.[7] While there is a reasonable general correspondence among states, specific levels can shift in relative energy by as much as 1.5 eV between these techniques.

Thus far the discussion has considered only the information derived from binding energies in a photoelectron spectrum. However, the intensity profile of a photoelectron peak as a function of input photon energy and angular detection also provides electronic and geometric structure information. The intensity of a photoelectron peak is determined by the photoionization cross section $\sigma_{if}(E_k)$ for ejection of an electron with kinetic energy, E_k, from the *nl* subshell,

$$\sigma_{if}(E_k) = 4\pi^2\alpha a_0^2/3g(h\nu)\left[\int \Psi_i \, \mathbf{r} \, \Psi_f \, d\tau\right]^2 \qquad \text{(VI-3)}$$

where α is the fine structure constant ($=1/137$), a_0 is the Bohr radius (0.529 Å), g is the number of degenerate subshells, and $h\nu$ is the

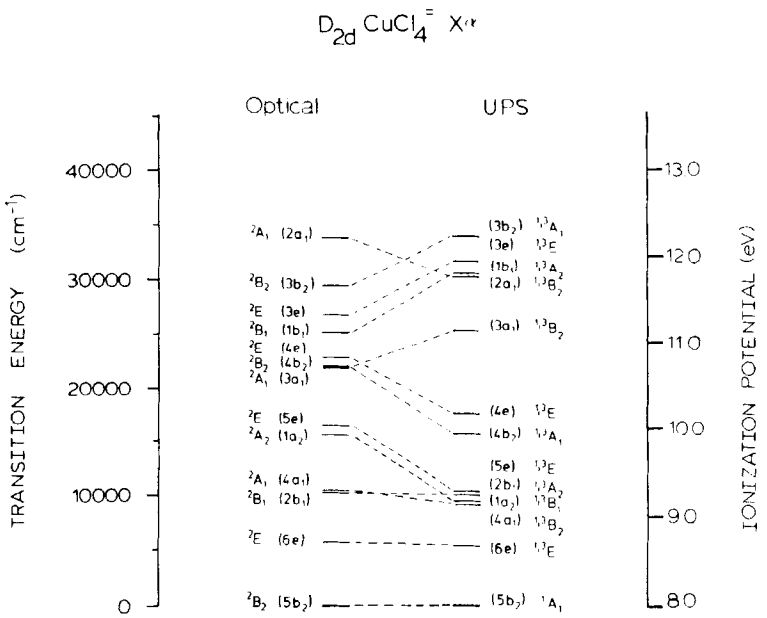

FIGURE VI-4 SCF-Xα-SW transition state calculations of the electronic absorption and UPS spectra of D_{2d}–$CuCl_4^=$. The ground state of the complex ($^2B_2(5b_2)$) and the ionized complex ($^1A_1(5b_2)$) have been aligned.

input photon energy (in rydbergs).[8] The term in brackets which governs the intensity is again the electric dipole transition moment integral for a transition from the ground state (referred to as the initial state ψ_i) to the excited state (the final state, ψ_f). In UPS, ψ_f includes both the ionized complex and the outgoing photoelectron. Assuming no orbital relaxation, the integral in Eq. (VI-3) involves only the wavefunction of the electron before (Φ_i, bound orbital) and after (Φ_f, continuum function) ionization. Photoionization cross-sections are usually treated on an atomic level, where both Φ_i and Φ_f are described by spherical harmonics with separable radial functions [initial orbital ϕ_{n,l,m_l}; photoelectron $\Phi_{E_k,l',m_{l'}}$].

Considering first the angular parts of the wavefunction, the selection rules which derive from the electric dipole operator in Eq. (VI-3) require that $l' = l \pm 1$. These are referred to as the channels of photoionization where the $l + 1$ channel is usually the dominant process. Hence, photoemission of an electron from a d orbital will

produce an f state continuum wavefunction. This in turn will produce an angular distribution ($d\sigma/d\Omega$) in the photoionization cross section which can be detected through angle resolved photoelectron spectroscopy.[10] The theoretical angular distribution for a photoelectron emitted from a Cu $3d_{x^2-y^2}$ orbital by z polarized light with $h\nu = 40$ eV is shown[10a] in Figure VI-5. Knowledge of these characteristic angular distributions (for example, in studies of chemisorbed small molecules on single crystal surfaces) has provided geometric structure information not available previously.[10,11]

In addition to angular variation, the photoionization cross-section also changes significantly with input photon energy as determined by the radial wavefunctions of the initial and final states.[9,12] As the photon energy increases, the kinetic energy of the ejected electron also increases. This causes the radial wavefunction of the continuum state to change in a manner which can be qualitatively described by its deBroglie wavelength ($\lambda_e(\text{Å}) = 12.3/\sqrt{E_K(\text{eV})}$) as shown in Figure VI-6. Quantitatively, the radial wavefunction for Φ_f must be obtained by solving the radial Schrödinger equation, which significantly modifies the continuum wavefunction (relative to a free electron) in the vicinity of the nucleus. There are two characteristic features of photoionization cross sections. First, the cross-sections do not simply decrease monotonically with increasing photon energy

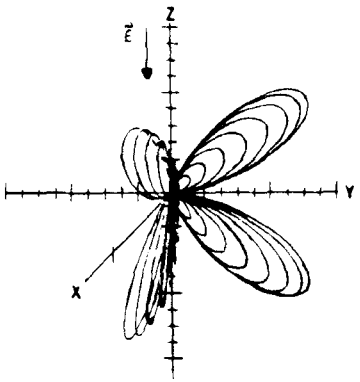

FIGURE VI-5 Angular distribution of photoelectron emission from a Cu $3d_{x^2-y^2}$ orbital: z polarized light with $h\nu = 40$ eV (taken from Ref. 10a). The three-dimensional plot in one quadrant is shown, but the full four quadrant cross sections can be obtained by reflection in the xz and yz planes.

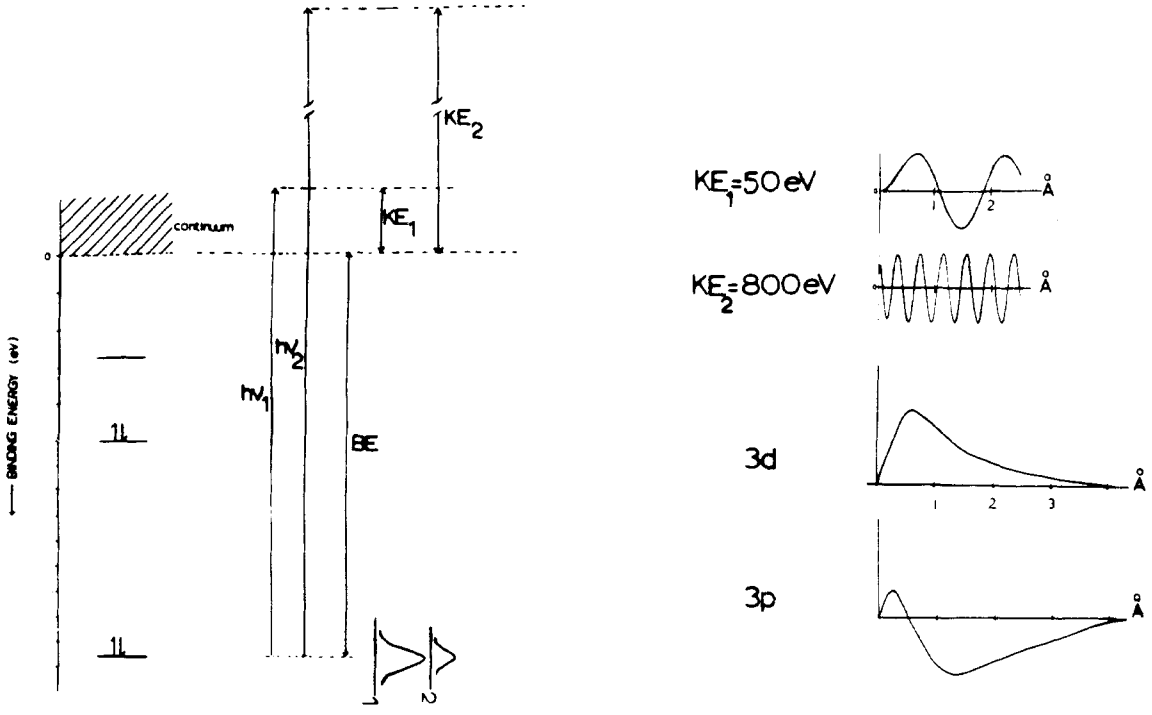

FIGURE VI-6 Photon energy dependence of the photoionization cross section: Intensity of photoelectron peak varies depending upon input photon energy, due to the variation in deBroglie wavelength of outgoing photoelectrons. These wavelengths are compared to the radial wavefunctions of Cu 3*d* and Cl 3*p* orbitals (right).

above the ionization threshold but in fact exhibit delayed maxima which depend on the l value of the orbital from which the electron is ejected.[9,12] As the l value of the orbital increases, the delayed maximum in photoelectron intensity shifts to higher energy above threshold and its magnitude decreases. This is caused by a repulsive centrifugal potential in the radial Schrödinger equation which depends on l' ($= l + 1$) for the continuum state. This tends to keep the radial part of the continuum wavefunction very small in the vicinity of the initial orbital wavefunction, resulting in limited overlap and thus low photoelectron intensity. As the E_k of the photoelectron increases, the continuum wavefunction penetrates this centrifugal barrier resulting in better overlap with the initial orbital wavefunction and thus greater intensity. The energy dependence of the photoionization cross-section of Cu $3d$ and Cl $3p$ orbitals[13] are given in Figure VI-7. The magnitude of the Cl 3p($l = 1$) photoionization cross-section is high near threshold, while that of Cu $3d(l = 2)$ has a delayed maximum of lower magnitude at ~50 eV above threshold.

The second important feature is illustrated in the photoionization cross-section of Cl $3p$ in Figure VI-7. The intensity drops rapidly to

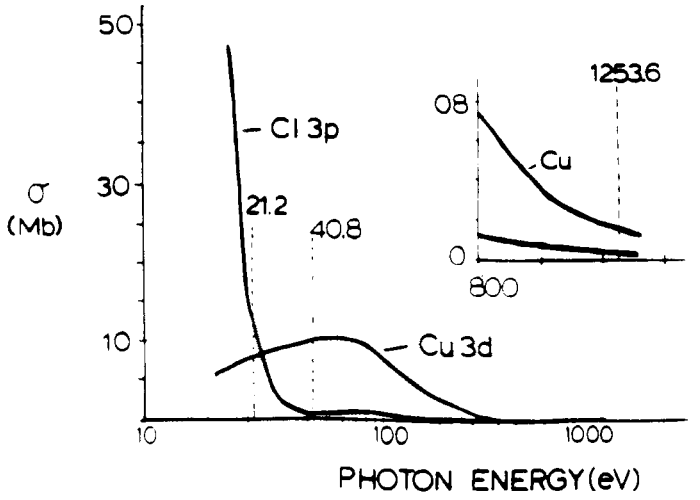

FIGURE VI-7 Energy dependence of atomic photoionization cross sections of Cu $3d$ and Cl $3p$ orbitals: Dashed lines indicate the He I, He II and Mg $K\alpha$ sources. Insert gives high photon energy region at higher sensitivity. 1 mb = 10^{-18} cm^2 (adapted from Ref. 13).

a value close to zero at ~50 eV and then increases with higher photon energies. This is known as a Cooper minimum[9] and is due to the node in the $3p$ radial wavefunction. This minimum will be present in the photoionization cross-sections of all orbitals which contain radial nodes (number of radial nodes $= n - l - 1$). As the E_k of the electron increases, its wavelength decreases and thus its overlap with the Φ_i changes. For Cl $3p$ at ~50 eV the overlap of the continuum radial wavefunction with the $3p$ orbital (Figure VI-6) is such that there is effective cancellation of contributions of opposite sign to the electric dipole transition moment expression in Eq. (VI-3). With further increases in $h\nu$ the wavelength of the radial wavefunction of the electron decreases and cancellation no longer occurs. For orbitals without radial nodes, the integral cannot change sign and thus will not exhibit this effect.

B. The Experiment

Several points concerning photoelectron spectroscopy on solids should be mentioned. First, in contrast to photons which can penetrate thousands of angstroms into a crystal, the average escape depth of an electron is quite small and depends on its kinetic energy[14] as shown in Figure VI-8. Thus, for kinetic energies between 10 and 1000 eV this technique is very surface sensitive and provides a powerful method for the study of the coordination chemistry of clean surfaces. Alternatively, if one is interested in using PES to study bulk properties of a solid material (in particular its electronic structure) one must be extremely careful to preclude the possibility of surface impurities or deviations in composition compared to that of the bulk. Another experimental detail worth noting is that photoelectron spectroscopy on insulating materials can often be complicated due to charging effects. Charging occurs because the photoelectric current leaving the surface creates a positive charge that cannot be readily neutralized by the bulk material. Thus PES peaks appear at deeper binding energy and are often broadened making binding energy determination difficult. To overcome this charging, a low energy flood of electrons is directed at the insulating surface. Binding energies must then be determined by careful referencing.

The variable photon energy photoelectron spectra of the valence level region of Cu(I) and Cu(II) chlorides[15] are given in Figure VI-9. For $Cu(I)Cl_4^{3-}$ in CuCl two peaks are observed, separated by ~3.5

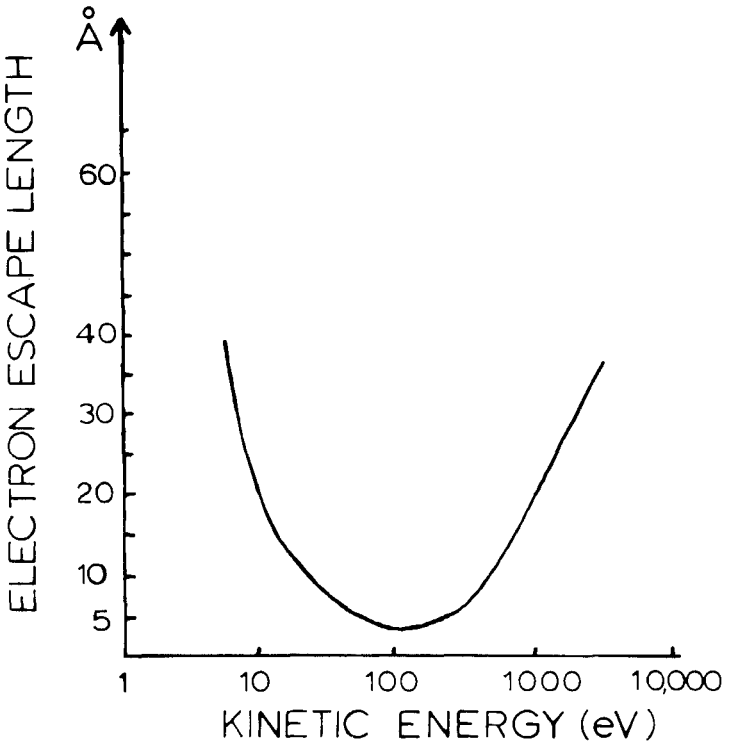

FIGURE VI-8 Average escape depth of an electron as a function of its kinetic energy. (Adapted from Ref. 14.)

eV. The peak to deeper binding energy is most intense in the $h\nu$ = 21.2 eV UPS spectrum. As the photon energy increases, this peak decreases in intensity relative to the peak at lower binding energy, reaching a minimum in the $h\nu$ = 48.4 eV spectrum and then increasing slowly with higher photon energy. This is just the behavior predicted from the photoionization cross sections for Cu 3*d* and Cl 3*p* given in Figure VI-7 and allows a definitive spectral assignment as indicated in Figure VI-9. It should be noted that UPS does not produce resolvable photoelectron peaks from individual Cu 3*d* (or Cl 3*p*) levels, but instead a composite band consisting of photoemission from all the 3*d* (or 3*p*) levels is observed.

For D_{2d}–Cu(II)Cl_4^- in Cs_2CuCl_4, two composite peaks again appear in the UPS spectrum. The higher binding energy peak shows

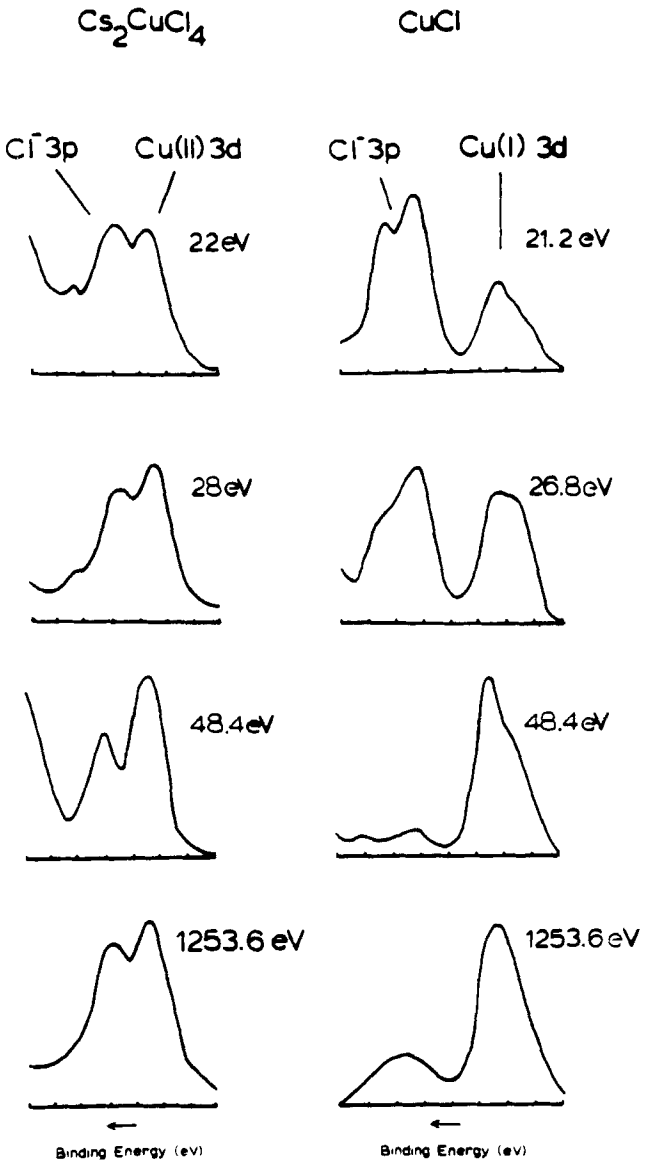

FIGURE VI-9 Variable photon energy photoelectron spectra of the valence level region of D_{2d}-$Cu(II)Cl_4^{=}$ and T_d-$Cu(I)Cl_4^{-3}$.

TABLE VI-1
Experimental and SCF-Xα-SW theoretical estimates of covalent mixing in Cu(I) and Cu(II) chlorides

	Cu(II)	Cu(I)
Experimental values:	65±7% Cu 3*d*	85±7% Cu 3*d*
Xα theoretical values:	50% (avg) Cu 3*d*	84% (avg) Cu 3*d*

	D_{2d} $Cu(II)Cl_4^{2-}$					D_{2d} $Cu(I)Cl_4^{3-}$				
		Binding energy (eV)	Percent Cu 3*d*	Percent Cl 3*p*	Percent other		Binding energy (eV)	Percent Cu 3*d*	Percent Cl 3*p*	Percent other
3*d*	$5b_2$	−4.6	45.9	51.9	2.1 Cu *p*	3*d*	$5b_2$	−3.2	73.1	25.5	1.4 Cu *p*
	$6e$	−5.3	46.7	50.9	2.3 Cu *p*		$6e$	−3.7	81.6	17.2	1.2 Cu *p*
	$2b_1$	−5.8	56.7	43.3			$2b_1$	−4.0	89.5	10.5	
	$4a_1$	−5.8	46.1	53.9			$4a_1$	−4.1	90.4	9.6	
3*p*	$1a_2$	−6.0	0.0	100.0		3*p*	$1a_2$	−6.0	0.0	100.0	
	$5e$	−6.1	1.0	99.0			$5e$	−6.1	1.3	98.7	
	$4b_2$	−6.8	1.8	95.2	3.0 Cu *p*		$3a_1$	−6.7	10.9	89.1	
	$4e$	−7.1	7.4	88.8	3.8 Cu *p*		$4b_2$	−6.8	5.3	93.3	1.4 Cu *p*
	$3a_1$	−7.2	57.5	40.3	2.0 Cu *s*		$4e$	−6.9	15.4	84.6	
	$1b_1$	−7.7	54.4	45.6			$1b_1$	−7.1	13.7	86.3	
	$3e$	−7.9	51.7	46.3	2.0 Cu *p*		$3b_2$	−7.2	26.2	70.2	3.6 Cu *p*
	$3b_2$	−8.2	56.6	42.4	1.0 Cu *p*		$3e$	−7.2	8.0	85.4	6.6 Cu *p*
	$2a_1$	−8.5	7.1	73.8	18.6 Cu *s*		$2a_1$	−8.2	2.2	79.7	18.0 Cu *s*

qualitatively the same relative photon energy dependence of its photoionization cross section as is observed in $Cu(I)Cl_4^{3-}$. However, for $Cu(II)Cl_4^{=}$ the Cu $3d$ and Cl $3p$ bands overlap significantly and the relative intensity changes with photon energy are much less pronounced. This requires significant mixing of the Cu $3d$ with the Cl $3p$ orbitals in the molecular wavefunctions of $CuCl_4^{=}$.

C. Comparison of Experiment and Theory

The atomic photoionization cross-sections given in Figure VI-7 can be used in conjunction with the UPS spectra in Figure VI-9 to estimate the covalent mixing of the $3d$ orbitals on the Cu with the $3p$ orbitals on the chlorides, averaged over the d orbitals.[15] The experimentally determined values for this mixing are given in Table VI-1. For $Cu(II)Cl_4^{=}$ the d levels are estimated to have ~65% d character with ~35% delocalization onto the chloride ligands, consistent with the higher resolution results obtained for the $d_{x^2-y^2}$ orbital from EPR spectroscopy (Section II). In $Cu(I)Cl_4^{3-}$ the d levels have 85% Cu d orbital character.[15,16] Apparently, the smaller energy difference between the Cu $3d$ and Cl $3p$ bands in $Cu(II)Cl_4^{=}$ (Figure VI-9) leads to a greater mixing among orbitals, as might be expected from one electron molecular orbital theory.

These results can be compared to those obtained from SCF-Xα-SW calculations which are also given in Table VI-1. For $Cu(I)Cl_4^{3-}$, the $3d$ and $3p$ bands are calculated to the split by ~3.5 eV, leading to an average mixing of ~15% Cl $3p$ character into the Cu $3d$ levels, in good agreement with the UPS experiment. For $Cu(II)Cl_4^{=}$, the separation between the Cu $3d$ and Cl $3p$ levels is calculated to be small (2 eV), producing 50% mixing of the orbitals, which is 15% greater than that obtained from experiment. Thus, these SCF-Xα-SW calculations produce a reasonable description of the bonding in copper chloride complexes but with some overestimate of the covalency in the case of cupric chloride.

References

1. In Section VI, only the D_{2d}–$CuCl_4^{=}$ complex in Cs_2CuCl_4 is considered. The results for D_{4h}–$CuCl_4^{=}$ are similar but the photoelectron spectra are more complicated due to overlap of features from the organic counterions.

2. (a) K. Siegbahn, C. Nordling, A. Fahlman, R. Nordberg, K. Hamrin, J. Hedman, G. Johansson, T. Bergmark, S. E. Karlsson, I. Lindgren, and B. Lindberg, *ESCA, Atomic, Molecular and Solid State Structure by Means of Electron Spectroscopy* (Almqvist and Wiksell, Uppsala, 1967).
(b) K. Siegbahn, C. Nordling, G. Johansson, J. Hedman, P. Hedan, K. Hamrin, U. Gelius, T. Bergmark, L. Werne, R. Manne, and Y. Baer, *ESCA Applied to Free Molecules* (North Holland, Amsterdam, 1969).
(c) C. R. Brundle and A. D. Baker, *Electron Spectroscopy, Theory, Techniques and Applications,* (Academic Press, London, 1977), Vol. 1.
(d) W. L. Jolly, Coord. Chem. Rev. **13**, 47 (1974).
3. (a) D. C. Frost, A. Ishitani, and C. A. McDowell, Mol. Phys. **24**, 861–877 (1972).
(b) S. L. Cohen and E. I. Solomon, unpublished results.
4. D. A. Shirley, in *Photoemission in Solids,* edited by M. Cardona and L. Ley (Springer Verlag, Berlin, 1978), Vol. I.
5. S. Hufner, in *Photoemission in Solids,* edited by M. Cardona and L. Ley (Springer Verlag, Berlin, 1978), Vol. II.
6. (a) D. W. Turner, C. Baker, A. D. Baker, and C. R. Brundle, *Molecular Photoelectron Spectroscopy* (John Wiley & Sons, London, 1970).
(b) J. W. Rabalais, *Principles of Ultraviolet Photoelectron Spectroscopy* (John Wiley & Sons, New York, 1977).
(c) I. Lindau and W. E. Spicer, in *Synchrotron Radiation Research,* edited by H. Winick, and S. Doniach (Plenum Press, New York, 1980).
(d) C. Furlani and C. Cauletti, Struc. Bonding, **35**, 119 (1978).
7. S. R. Desjardins, K. W. Penfield, S. L. Cohen, R. L. Musselman, and E. I. Solomon, J. Am. Chem. Soc. **105**, 4590–4603 (1983).
8. It should be noted that the photoionization cross section is directly proportional to the absorption spectrum for a transition into the continuum (see Ref. 9).
9. U. Fano and J. W. Cooper, Rev. Mod. Phys. **40**, 441 (1968).
10. (a) S. M. Goldberg, C. S. Fadley, and S. Kono, J. Electron. Spec. Relat. Phen. **21**, 285 (1981).
(b) E. W. Plummer and W. Eberhardt, Adv. Chem. Phys. **49**, 533 (1983).
(c) E. W. Plummer and T. Gustafsson, Science **198**, 165 (1977).
11. (a) M. J. Sayers, M. R. McClellan, R. R. Gay, E. I. Solomon, and F. R. McFeely, Chem. Phys. Lett. **75**, 575 (1980).
(b) M. R. McClellan, M. Trenary, N. S. Shinn, M. F. Sayers, K. L. D'Amico, E. I. Solomon, and F. R. McFeely, J. Chem. Phys. **74**, 4726 (1981).
(c) K. L. D'Amico, M. Trenary, N. D. Shinn, E. I. Solomon, and F. R. McFeely, J. Am. Chem. Soc. **104**, 5102 (1982).
12. (a) S. T. Manson, in *Photoemission in Solids,* edited by M. Cardona and L. Ley (Springer Verlag, Berlin, 1978), Vol. I.
(b) D. E. Eastman, M. Kuznietz, J. Appl. Phys. **42**, 1396 (1971).
13. Juo Ming Yeh, unpublished results.
14. I. Lindau and W. E. Spicer, J. Electron. Spectrosc. Relat. Phenon. **3**, 409 (1974).
15. S. L. Cohen, S. V. Didziulis, and E. I. Solomon, manuscript in preparation.
16. (a) A. Goldman, J. Tejeda, N. J. Shevchick, and M. Cardona, Phys. Rev. B. **10**, 4388 (1974).
(b) S. Kono, T. Ishii, T. Sagawa, T. Kobayasi, Phys. Rev. B, **8**, 995 (1973).